Covalent linkage of nanodiamond-paclitaxel for drug delivery and cancer therapy

2010 Nanotechnology 21 315106

(http://iopscience.iop.org/0957-4484/21/31/315106)

Nanotechnology **21** (2010) 315106 (14pp) doi:10.1088/0957-4484/21/31/315106

Covalent linkage of nanodiamond-paclitaxel for drug delivery and cancer therapy

Kuang-Kai Liu[1], Wen-Wei Zheng[2], Chi-Ching Wang[1], Yu-Chung Chiu[3], Chia-Liang Cheng[3,4], Yu-Shiu Lo[2], Chinpiao Chen[2,4] and Jui-I Chao[1,4,5]

[1] Department of Biological Science and Technology, National Chiao Tung University, Hsinchu 30013, Taiwan
[2] Department of Chemistry, National Dong Hwa University, Hualien 97401, Taiwan
[3] Department of Physics, National Dong Hwa University, Hualien 97401, Taiwan

E-mail: clcheng@mail.ndhu.edu.tw, chinpiao@mail.ndhu.edu.tw and jichao@faculty.nctu.edu.tw

Received 12 April 2010, in final form 14 June 2010
Published 15 July 2010
Online at stacks.iop.org/Nano/21/315106

Abstract

A nanoparticle-conjugated cancer drug provides a novel strategy for cancer therapy. In this study, we manipulated nanodiamond (ND), a carbon nanomaterial, to covalently link paclitaxel for cancer drug delivery and therapy. Paclitaxel was bound to the surface of 3–5 nm sized ND through a succession of chemical modifications. The ND-paclitaxel conjugation was measured by atomic force microscope and nuclear magnetic resonance spectroscopy, and confirmed with infrared spectroscopy by the detection of deuterated paclitaxel. Treatment with 0.1–50 μg ml^{-1} ND-paclitaxel for 48 h significantly reduced the cell viability in the A549 human lung carcinoma cells. ND-paclitaxel induced both mitotic arrest and apoptosis in A549 cells. However, ND alone or denatured ND-paclitaxel (after treatment with strong alkaline solution, 1 M NaOH) did not induce the damage effects on A549 cells. ND-paclitaxel was taken into lung cancer cells in a concentration-dependent manner using flow cytometer analysis. The ND-paclitaxel particles were located in the microtubules and cytoplasm of A549 cells observed by confocal microscopy. Furthermore, ND-paclitaxel markedly blocked the tumor growth and formation of lung cancer cells in xenograft SCID mice. Together, we provide a functional covalent conjugation of ND-paclitaxel, which can be delivered into lung carcinoma cells and preserves the anticancer activities on the induction of mitotic blockage, apoptosis and anti-tumorigenesis.

(Some figures in this article are in colour only in the electronic version)

1. Introduction

Cancers have become the leading cause of death in the world. Among all, lung cancer is one of the most-often causes and occurrences that leads to the mortality. Although treatment of cancers include surgery, radiation and chemotherapy, patients in the late stage are usually managed primarily with chemotherapy. Unfortunately, poor intracellular uptake, limited circulation stability and normal cell damages reduce the abilities of chemotherapeutic drugs. Nanoparticles provide the opportunity for improving cancer therapeutics by conjugating drugs or biological molecules to improve the treatments [1–4]. For example, carbon nanotubes have been used as a carrier for cancer drug delivery that effectively inhibit tumor growth in mice [5]. Nanoliposomal-carrying cancer drugs have been successfully used in cancer therapy,

[4] Authors to whom any correspondence should be addressed.
[5] Address for correspondence: Department of Biological Science and Technology, National Chiao Tung University, 75, Bo-Ai Street, Hsinchu 30013, Taiwan.

demonstrating the benefits of prolonged tissue residence and reduced toxicity [6–8].

The issue of potential toxicity of nanomaterials has been the major concern, although nanoparticles were intensively developed for biomedical applications [9, 10]. A non-toxic and biocompatible nanomaterial is required for clinical use. It has been shown that nanodiamond (ND) particles did not induce significant cytotoxicity in a variety of cell types including lung [11, 12], neuronal [13], renal [14, 15] and cervical cells [16]. In addition, cell division and differentiation were not altered following ND treatment [12]. Recently, the intravenous injection of ND particles into mice did not significantly induce symptoms of abnormality [17]. As a result, ND is a relative safe nanomaterial based on its non-cytotoxicity and biocompatibility; however, further rigorous evaluation before clinical applications is needed. Moreover, ND is a detectable nanomaterial using its fluorescence property but without photobleaching [12, 14, 18]. It has also been shown that ND can be used for the labeling and tracking of cancer cells [12]. Accordingly, the properties of biocompatible and detectable ND are very useful for biomedical applications.

The surface of ND particles can also be a unique platform for the conjugation of chemicals and biomolecules after functional modifications [18–23]. ND particles provide two strategies of conjugation by covalent or non-covalent bonding of chemicals and biomolecules. The modified ND surfaces have been shown to conjugate with DNA [19, 20], lysozyme [18], cytochrome c [21], growth hormone [22], biotin [23], alpha-bungarotoxin [24] and insulin [25]. Lysozyme and alpha-bungarotoxin proteins can be adsorbed on the surface of carboxylated ND via non-covalent bonding while still preserving the biological activities of these proteins [18, 24]. The hydrogel of ND with chemotherapeutic drugs such as doxorubicin was developed for drug delivery by non-covalent adsorption [26]. However, the covalent linking of cancer drugs to ND particles and their anticancer activities are poorly understood.

In this study, we create a novel covalently bonded ND-paclitaxel conjugate for drug delivery and cancer therapy. ND-paclitaxel can be taken into human lung carcinoma cells. Interestingly, ND-paclitaxel displayed anticancer activities by inducing mitotic arrest and apoptosis. This is the first time to demonstrate that ND-paclitaxel inhibits the tumorigenesis of human lung cancer cells in xenograft SCID mice but ND alone did not induce the effects on mitotic arrest, apoptosis and anti-tumorigenesis. Our study indicates the functional linkages of drugs or biomolecules with ND may be developed for varying biomedical applications.

2. Experimental details

2.1. Chemicals and reagents

Paclitaxel was purchased from Tokyo Chemical Industry Co. (Ltd Japan). Succinic anhydride, triethylamine and EEDQ (2-ethoxy-1-ethoxycarbonyl-1,2-dihydroquinoline) were purchased from Acros Organics (Geel, Belgium). Powdered ND particles with diameters of 3–5 nm were purchased from Nanostructured and Amorphous Materials Inc. (Houston, TX). Hoechst 33258, 3-(4,5-dimethyl-thiazol-2-yl) 2,5-diphenyl tetrazolium bromide (MTT) and the Cy3-labeled mouse anti-β-tubulin (c-4585) were purchased from Sigma Chemical Co. (St Louis, MO). Anti-CDC2 and anti-phospho-CDC2 were purchased from Cell Signaling Technology Inc. (Beverly, MA). Anti-actin (I-19) was purchased from Santa Cruz Biotechnology, Inc. (Santa Cruz, CA).

2.2. Preparation of ND-paclitaxel

The chemical synthetic procedure for the conjugation of ND and paclitaxel has been shown in scheme 1. Initial chemical treatment of ND powders (**1**) by carboxylation was carried out according to standard procedures. The ND particles were stirred in a 3:1 (v/v) mixture of concentrated HCl and HNO_3 at room temperature for three days, then diluted with deionized H_2O and separated by centrifugation at 900 rpm. After centrifugation, the pellets were extensively rinsed with deionized H_2O three times. Thereafter, ND particles were heated in 0.1 M NaOH solution at 90 °C for 2 h. The ND particles were again heated in 0.1 M HCl at 90 °C for 2 h. The resulting carboxylated ND (**2**) was dried under vacuum for 24 h. A mixture of ND–$(CO_2H)_x$ and THF was sonicated under argon for 5 min. After this time, $LiAlH_4$ was added and the system was refluxed for 24 h. The reaction mixture was cooled to room temperature and quenched with deionized H_2O. The supernatant liquid was removed by centrifugation at 900 rpm and the residue was rinsed with deionized H_2O three times. The residue was then heated in 6 M NaOH at 90 °C overnight. The reaction mixture was cooled to room temperature, washed and treated with 0.1 M HCl as described earlier. The repeatedly washed ND–$(CH_2OH)_n$ (**3**) was dried under vacuum at 50 °C. To the ND–$(CH_2ONa)_n$ mixture generated from (**3**) and NaH in THF was added 6-(chloro-hexyloxy)-tetrahydropyran and the mixture was stirred at 45 °C for 24 h. The reaction mixture was cooled to room temperature, washed with THF and water as before, and finally dried under a vacuum. A suspension of ND–$(CH_2O(CH_2)_6OTHP)_x$ (**4**) in MeOH/H_2O (3:1) was sonicated for 5 min; p-TsOH was then added until the solution became acidic, after which it was stirred at room temperature overnight. The reaction mixture was worked-up as described earlier to generate (**5**) as a dry powder. Triethylamine was added to a slurry of ND–$(CH_2O(CH_2)_6OH)_x$ (**5**) in THF at 0 °C and the mixture was stirred under argon for 30 min. Methanesulfonyl chloride was then added dropwise and the resulting mixture was stirred at 0 °C for 1 h and at room temperature overnight. Deionized H_2O was added and the centrifuged residue was washed repeatedly with THF, water and finally dried under a vacuum to yield ND–$(CH_2O(CH_2)_6OMs)_x$ (**6**). ND–$(CH_2O(CH_2)_6OMs)_x$ (**6**) was suspended in DMF and sonicated under argon for 5 min; NH_4OH was then added and the mixture was again sonicated for 3 min. It was then stirred at 70 °C for 12 h. The reaction mixture was cooled to room temperature and rinsed with THF three times and deionized H_2O twice. Separation by centrifugation at 900 rpm yielded ND–$(CH_2O(CH_2)_6NH_2)_x$ (**7**), which was then dried under a vacuum.

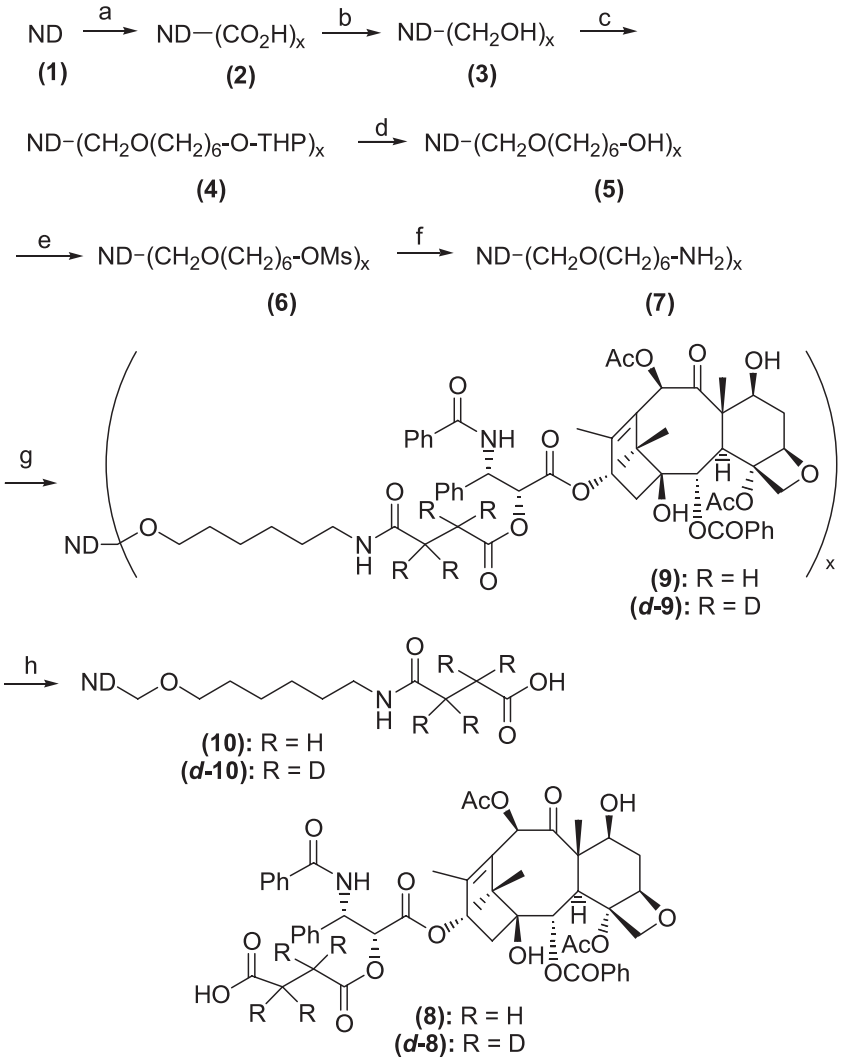

Scheme 1. Chemical synthesis of ND-paclitaxel. The chemical products are indicated by the numbers. The succession of chemical synthetic processes is the following: (a) HCl/HNO_3 (3:1), rt, 3 d; 1 M NaOH, 90 °C, 2 h; 1 M HCl, 90 °C, 2 h; (b) $LiAlH_4$, THF, reflux 24 h; 6 M NaOH, 90 °C, overnight; (c) NaH, THF, THP–O–$(CH_2)_5CH_2Cl$; (d) p-TsOH, MeOH/H_2O (3:1), rt, overnight; (e) MsCl, Et_3N, THF, 0 °C, 1 h, rt, overnight; (f) NH_4OH(aq), reflux, 24 h; (g) 8 (paclitaxel-2′-succinate), EEDQ, Et_3N, CH_2Cl_2, rt, 3 h; (h) 1 M NaOH, rt, overnight.

Paclitaxel-2′-succinate (**8**) was prepared according to the known procedure [27]. EEDQ was added to a solution of paclitaxel-2′-succinate (**8**) in dry CH_2Cl_2 and stirred for 30 min at room temperature. To this was added an ultrasonicated suspension of (**7**) and Et_3N in CH_2Cl_2. The resulting mixture was sonicated for an additional 5 min and stirred at room temperature for 3 h. Paclitaxel-conjugated ND (**9**) was separated by centrifugation at 900 rpm and then rinsed three times with CH_2Cl_2, three times with THF and twice with deionized H_2O; the system was then separated by centrifugation at 900 rpm. The resulting pellet was transferred to a round flask using a small amount of deionized H_2O and dried under a vacuum to give paclitaxel-conjugated ND (**9**) as a dry gray powder. The basic hydrolysis of (**9**) was performed by treating with a 1 M solution of sodium hydroxide, sonicating for 5 min and stirring overnight at room temperature. The Paclitaxel-hydrolyzed-ND (**10**) thus obtained was separated by centrifugation at 900 rpm, rinsed with THF three times and deionized H_2O twice, and dried under a vacuum.

2.3. Fourier transform infrared (FTIR) spectroscopy

ND and ND derivatives were analyzed using a Fourier transform infrared spectrometer (Bomem, MB154, Canada) with samples placed in a vacuum environment ($\sim 10^{-6}$ Torr) for characterization of various functional groups of the prepared samples deposited on an Si wafer surface. Typically, the spectra were collected with 4 cm^{-1} nominal resolution and 200 scans for each spectrum in a direct single-path configuration. A background spectrum of blank Si wafer was collected each time for background correction.

2.4. Atomic force microscopy (AFM)

For AFM measurements, ND powders were suspended in dichloromethane by ultrasonication with a concentration of $\sim$5 mg ml^{-1} and centrifugation at 10 000 rpm for 10 min. 30 μl of the supernatant solution was placed on a glass substrate (1.5 cm × 1.5 cm) followed by a two-step spin-coating

process: 3000 rpm for 10 s, then 4000 rpm for 20 s. The AFM images shown were obtained using an Autoprobe CP-Research (Veeco, USA) in tapping mode. Silicon nitride cantilevers from Nanosensors (type PPP-RT-NCHR) with a nominal force constant of 42 N m^{-1} and resonant frequency of ∼330 kHz were used.

2.5. Nuclear magnetic resonance (NMR) spectroscopy

The chemical products were analyzed by NMR spectroscopy. The dried sample was suspended in $CDCl_3$ (0.6 ml) and used the regular methods to scan overnight. The samples were analyzed by NMR spectroscopy analysis (^{1}H NMR, Bruker Avance 400 MHz spectrometer).

2.6. Cell culture

The A549 lung cancer cell line (ATCC #CCL-185) was from the American Type Culture Collection (Manassas, VA, USA) that was derived from the lung adenocarcinoma of a 58 year-old Caucasian male. A549 cells were maintained in complete RPMI-1640 medium (Invitrogen Co., Carlsbad, CA), which contained 10% fetal bovine serum, 100 units ml^{-1} penicillin and 100 μg ml^{-1} streptomycin. These cells were incubated at 37 °C and 5% CO_2 in a humidified incubator (310/Thermo, Forma Scientific, Inc., Marietta, OH).

2.7. Cell viability assay

In our experiments, the powders of ND or ND-paclitaxel were prepared with sterilized distilled water in laminar flow. To avoid aggregation, the samples were ultrasonicated for 20 min at room temperature before use. In addition, the samples need to be freshly prepared. Briefly, the cells were plated in 96-well plates at a density of 1×10^4 cells/well for 16–20 h. The cells were treated with ND or ND-paclitaxel for 48 h in complete medium. After treatment, the medium was replaced and the cells were incubated with 0.5 mg ml^{-1} of MTT in complete medium for 4 h. The surviving cells converted MTT to formazan, generating a blue–purple color when dissolved in dimethyl sulfoxide. The intensity was measured at 565 nm using a plate reader (Molecular Dynamics, OPTImax). The cell viability was calculated by dividing the absorbance of the treated cells by that of the untreated cells.

2.8. Confocal microscopy

The cells were cultured on cover slips and kept in a 35 mm Petri dish for 16–20 h before treatment. After treatment with or without ND, ND-paclitaxel or paclitaxel, the cells were washed with isotonic PBS (pH 7.4) and then were fixed with 4% paraformaldehyde solution in PBS for 1 h at 37 °C. Thereafter, the cover slips were washed three times with PBS, and non-specific binding sites were blocked with PBS that contained 10% FBS and 0.3% Triton X-100 for 1 h. The nuclei and β-tubulin were stained with Hoechst 33258 and the Cy3-labeled anti-β-tubulin (Sigma Chemical Co.), respectively. At the end of staining, the samples were examined under a confocal laser scanning microscope (Leica TCS SP2, Mannheim, Germany). The fluorescence images were displayed using the frames stored in the computer and the images were merged by software written for the Leica confocal microscope (Ver. Lite).

2.9. Fluorescence intensity of ND-paclitaxel in cells by flow cytometer

A549 cells were plated at a density of 7×10^5 cells per 60 mm Petri dish in complete medium for 16–20 h. Thereafter, the cells were treated with 0–50 μg ml^{-1} ND-paclitaxel for 48 h. After treatment with or without ND-paclitaxel, the cells were collected and fixed with ice-cold 70% ethanol overnight at −20 °C. The samples were analyzed by flow cytometer (FACSCalibur, BD Biosciences). A minimum of 10 000 cells were analyzed. The fluorescence from the ND-paclitaxel was excited at a wavelength of 488 nm and the emission was collected in the green light signal range. The fluorescence intensity was quantified by CellQuest software (BD Biosciences).

2.10. Cell cycle analysis

The cell cycle phases can be separated into G_0/G_1, S and G_2/M by flow cytometer analysis. To examine the effect of ND-paclitaxel on the cell cycle progression, A549 cells were plated at a density of 1×10^6 cells per 60 mm Petri dish in complete medium for 16–20 h. At the end of treatment, the cells were collected and fixed with ice-cold 70% ethanol overnight at −20 °C. Thereafter, the cell pellets were treated with 4 μg ml^{-1} propidium iodide solution containing 1% Triton X-100 and 100 μg ml^{-1} RNase for 30 min. To avoid cell aggregation, the cell solutions were filtered through a nylon mesh membrane. Finally, the samples were analyzed by a flow cytometer (FACSCalibur, Becton-Dickinson, San Jose, CA). At least 10 000 cells were analyzed for DNA content. The percentage of cell cycle phases was quantified by ModFit LT software (Ver. 2.0, Becton-Dickinson).

2.11. Mitotic index analysis

To determine whether G_2 or M phases increased by ND-paclitaxel, the cells were analyzed by mitotic index. The mitotic cells showed round-up morphology, compact chromosomes, spindle formation and contained an intact cell membrane but did not produce cell membrane blebbing or the formation of apoptotic bodies. The adherent cells were cultured on cover slips in a 60 mm Petri dish for 16–20 h before treatment. After treatment, the cells were carefully and gently washed with PBS (pH 7.4) to avoid the loss of mitotically rounded-up cells, and then fixed with 4% paraformaldehyde solution in PBS for 1 h at 37 °C. The β-tubulin was stained with the Cy3-labeled mouse anti-β-tubulin (1:50) for 30 min at 37 °C. Finally, the nuclei were stained with 2.5 μg ml^{-1} Hoechst 33258 for 30 min. The mitotic index indicated the percentage of mitotic cell number/total counted cells that was counted under a fluorescence microscope (Leica TCS SP2) in each treatment.

2.12. Apoptotic nuclear counting

After treatment with or without ND-paclitaxel, the cells were carefully and gently washed with isotonic phosphate-buffered saline (PBS) (pH 7.4) and fixed with 4% paraformaldehyde solution in PBS for 1 h at 37 °C. The β-tubulin was stained with the Cy3-labeled mouse anti-β-tubulin (1:50) for 30 min at 37 °C. The nuclei were stained with 2.5 μg ml^{-1} Hoechst 33258 for 30 min. The number of apoptotic nuclei were counted under a fluorescence microscope (Leica TCS SP2). The cell morphology of apoptosis was confirmed by the observation of nuclear fragmentation, cell membrane blebbing and cytoskeleton disruption. The apoptotic percentage (the apoptotic cell number/total counted cells $\times$100%) was counted under a fluorescence microscope (Leica TCS SP2) in each treatment.

2.13. Western blot analysis

Western analyses of phospho-CDC2, CDC2, and actin were performed using specific antibodies. After treatment with or without ND-paclitaxel, the cells were lysed in the ice-cold whole cell extract buffer containing the protease inhibitors as described [28]. Equal amounts of proteins in samples were subjected to electrophoresis using 12% sodium dodecyl sulfate-polyacrylamide gels. After electrophoretic transfer of proteins onto polyvinylidene difluoride membranes, they were sequentially hybridized with primary antibody and followed with a horseradish peroxidase-conjugated secondary antibody (Santa Cruz Biotechnology, Inc., Santa Cruz, CA). Finally, the protein bands were visualized using the enhanced chemiluminescence detection system (Perkin Elmer Life Sciences).

2.14. Human lung tumor xenograft in SCID mice

A lung carcinoma xenograft was developed in five-week-old CB17/Icr-Prkdc^{scid}/Crl mice that were obtained from BioLASCO (BioLASCO Taiwan Co., Ltd). A549 lung carcinoma cells were treated with or without 10 μg ml^{-1} ND-paclitaxel for 48 h. Thereafter, each mouse received 1×10^6 A549 cells (in 100 μl of sterile 1$\times$ PBS) by being injected subcutaneously into the right flank area. The tumor sizes in SCID mice were measured by a digital caliper every four days and calculated tumor volume by the following formula: (width^2 $\times$ length)/2. Finally, the visible lung tumors were separated from sacrificed xenograft mice.

2.15. Statistical analysis

Each experiment was repeated at least three times. Data were analyzed by two-way analysis of variance (ANOVA) and further *post-hoc* tests. A p value of <0.05 was considered statistically significant.

3. Results

3.1. Characterization of ND-conjugated paclitaxel

An ND-conjugated paclitaxel by covalent bonding was illustrated in figure 1(A). To examine the linkage of ND and paclitaxel, FTIR analysis was used for characterizing these ND derivatives. FTIR of the solid ND samples confirmed the successful functionalization of ND at various steps. The stretching of the specific functionalities of the intermediates—SO_2 (1203 and 1315 cm^{-1}), NH_2 (3390 cm^{-1}) (figure 1(B)(b) and inset (II); the green spectra are the spectral fits for the peaks observed) and CONH (1700 cm^{-1})—and their disappearances in the subsequent stages were clearly observed. As further proof of the conjugation of paclitaxel on the ND surface, deuterated paclitaxel-2′-succinate (scheme 1, (**d-8**)) was synthesized in a similar way as (**8**) and attached to the ND surface (scheme 1, (**d-9**)). (**d-9**) displayed intense bands around ~2131 and 2219 cm^{-1} that are characteristic of the C–D stretching frequency (figure 1(B)((c)–(e)) and inset (III)). Saponification of (**d-9**) cleaved paclitaxel from the ND surface at the ester linkage, leaving behind (**d-10**), which retained the C–D stretching frequencies in the IR spectrum (figure 1(B)(e) and inset (III)). In addition to FTIR analysis, we have further examined the particle size and surface topography of pristine ND (**1**) and ND-paclitaxel (**9**) by AFM. The average size (diameter) of the pristine ND particles was around 3–5 nm by AFM analysis (figure 1(C), left); however, the ND-paclitaxel particles were increased to ~10 nm (figure 1(C), right). The NDs after paclitaxel modification may have caused the whole composite (ND-paclitaxel) to aggregate as observed in our TEM studies (data not shown). This may be reflected in our AFM observation for the increased average sizes of the composite as the AFM reflects the surface morphological structures. Furthermore, we found that the ^{1}H-NMR spectrum of (**9**) displayed signals due to the paclitaxel moiety on the ND's surface as compared to the ND sample, showing the conjugation of paclitaxel on ND (**1**) (figure 1(D)).

3.2. ND-paclitaxel reduces cell viability in lung carcinoma cells

The cell viability of ND, ND-paclitaxel and NaOH-treated ND-paclitaxel on the A549 human lung carcinoma cells were analyzed by MTT assay. Figure 2(A) shows that treatment with 0.1–50 μg ml^{-1} ND particles for 48 h did not significantly induce the cytotoxicity of A549 cells. In contrast, ND-paclitaxel (0.1–50 μg ml^{-1} for 48 h) significantly reduced the cell viability in a concentration-dependent manner (figure 2(B)). The IC_{50} value (the concentration of 50% inhibition of cell viability) of ND-paclitaxel was around 1 μg ml^{-1} towards the A549 cells. Paclitaxel (10–100 nM for 48 h) also reduced the cell viability in A549 cells (figure 2(C)). To further prove the biological activity of paclitaxel on ND, ND-paclitaxel was treated with strong alkaline solution (1 M NaOH), which caused dysfunction of paclitaxel. Indeed, denatured ND-paclitaxel lost the activity to cause lung cancer cell death (figure 2(D)).

3.3. Uptake ability of ND-paclitaxel in lung carcinoma cells

We have examined the uptake ability of ND-paclitaxel in lung carcinoma cells by flow cytometer. Treatment with ND-paclitaxel (0.1–50 μg ml^{-1} for 48 h) elevated the green fluorescence intensities so that the spectra were shifted to the

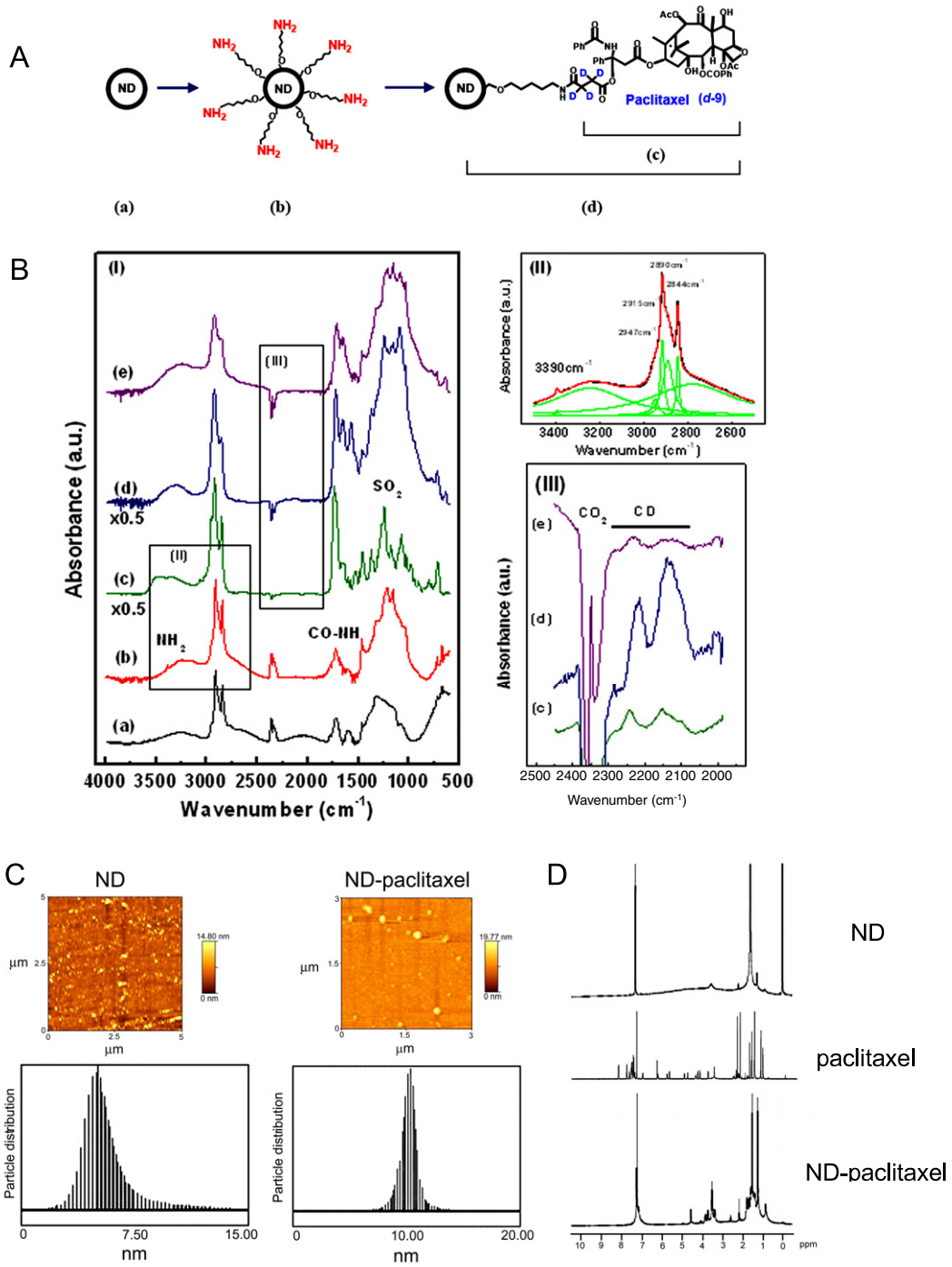

Figure 1. Characterization of ND-paclitaxel conjugation. (A) (a) ND of 3–5 nm (**1**); (b) ND derivative, ND–$(CH_2O–(CH_2)_6–NH_2)_x$ (**7**); (c) deuterated paclitaxel (**d-8**); (d) ND-deuterated paclitaxel (**d-9**). (B) Infrared spectra of each step of the synthesis process, (I) FTIR spectra of 3–5 nm ND and its derivatives taken in vacuum ($\sim 10^{-6}$ Torr): (a) 3–5 nm ND (**1**); (b) ND–$(CH_2O–(CH_2)_6–NH_2)_x$ (**7**); (c) deuterated paclitaxel (**d-8**); (d) ND-deuterated paclitaxel (**d-9**); (e) (**d-10**) ND-deuterated paclitaxel after treatment with 1 M NaOH. (II) The observed N–H stretching (~ 3390 cm^{-1}) from ND–$(CH_2O–(CH_2)_6–NH_2)_x$ in spectrum (b). The green spectra are the fits for the observed peaks. The prominent peaks from 2800–3000 cm^{-1} are from CH_x in the samples. (III) The enlarged section of the observed C–D stretching from the deuterated paclitaxel in spectra ((c), (d)) in the 2000–2400 cm^{-1} region. The broad peaks around 2350 cm^{-1} arise from variation in atmospheric CO_2 outside the vacuum chamber. The observation of both CD and NH ensure the products of each step are according to the designed scheme. (C) ND or ND-paclitaxel particles were coated on the mica slice and were observed by AFM. The deflection images from AFM show the contour and size of ND (left) and ND-paclitaxel (right). A histogram of height distribution in ND (left, blow) and ND-paclitaxel (right, below) were measured by AFM. ND and ND-paclitaxel were scanned from random fields (at least three times) in a 5 μm × 5 μm area under AFM. The data shown were from one of the scanned images. (D) The chemical products of ND (**1**), paclitaxel (**8**) and ND-paclitaxel (**9**) were analyzed by NMR spectroscopy. The dried sample was suspended in $CDCl_3$ (0.6 ml), and used the regular methods to scan overnight. The peaks of paclitaxel derivative were presented in the ND-paclitaxel NMR spectrum but not shown in the ND NMR spectrum. The peaks were assigned as follows: 1.4–1.9 (m, –CH_3, C–CH_2–C); 2.17 (s, –$OCOCH_3$); 2.6 (s, –$NCOCH_2CH_2COO$–); 3.4 (m, C–CH_2–NHCO–); 3.75, 3.85 (m, –C–CH_2–O–); 4.1 (m, CO_2CHR_2–); 4.95 (m, –CH_2– of cyclic ether (four-membered ring)); 7.17 (Ar–H).

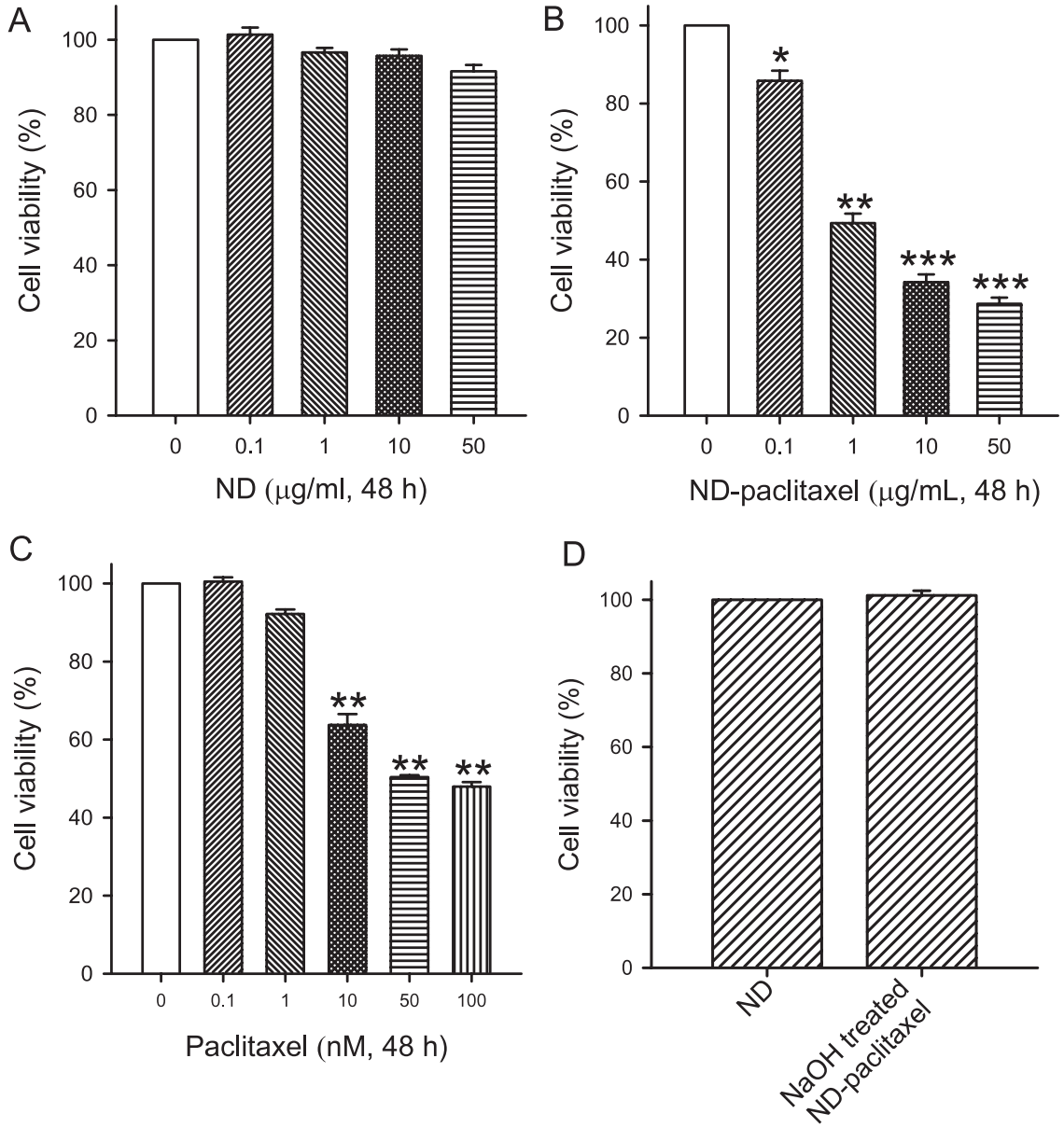

Figure 2. Effect of ND-paclitaxel on the cell viability in human lung carcinoma cells. (A) A549 cells were treated with or without ND (0.1–50 μg ml^{-1} for 48 h). (B) A549 cells were treated with or without ND-paclitaxel (0.1–50 μg ml^{-1} for 48 h). (C) A549 cells were treated with paclitaxel (0–50 nM for 48 h). At the end of treatment, the cell viability was measured by MTT assay. Results were obtained from 4–12 separate experiments and the bar represents mean ± S.E. $^{*}p < 0.05$, $^{**}p < 0.01$ and $^{**}p < 0.001$ indicate significant difference between control and ND-paclitaxel (or paclitaxel)-treated samples. (D) A549 cells were treated with 50 μg ml^{-1} ND particles or NaOH-treated ND-paclitaxel for 48 h. The cell viability was measured by MTT assay. Results were obtained from eight experiments and the *bar* represents mean ± S.E.

right in A549 cells (figure 3(A)). The quantified fluorescence intensities showed the uptake ability of ND-paclitaxel via a concentration-dependent manner in A549 cells (figure 3(B)). The fluorescence intensities were increased to 4–5-fold in A549 cells than untreated cells on treatment with 10–50 μg ml^{-1} ND-paclitaxel (figure 3(B)).

3.4. ND-paclitaxel blocks microtubules to induce abnormal mitotic cells

To examine whether ND-paclitaxel induced microtubule inhibition, A549 cells were treated with ND-paclitaxel and subjected to cytoskeleton and nuclear staining. The green fluorescence from the ND particles was excited by a wavelength of 488 nm and the emission was collected in the range 510–530 nm and the red color indicated the location of microtubules in A549 cells. Treatment with ND-paclitaxel or paclitaxel markedly increased the abnormal mitotic cell number (figure 4(A), stars). ND-paclitaxel or paclitaxel blocked spindle formation and chromosome segregation (figure 4(B)). The derangement of chromosomes was elicited by ND-paclitaxel or paclitaxel (figure 4(B), arrows). However, ND particles did not induce the aberrant chromosomes in the

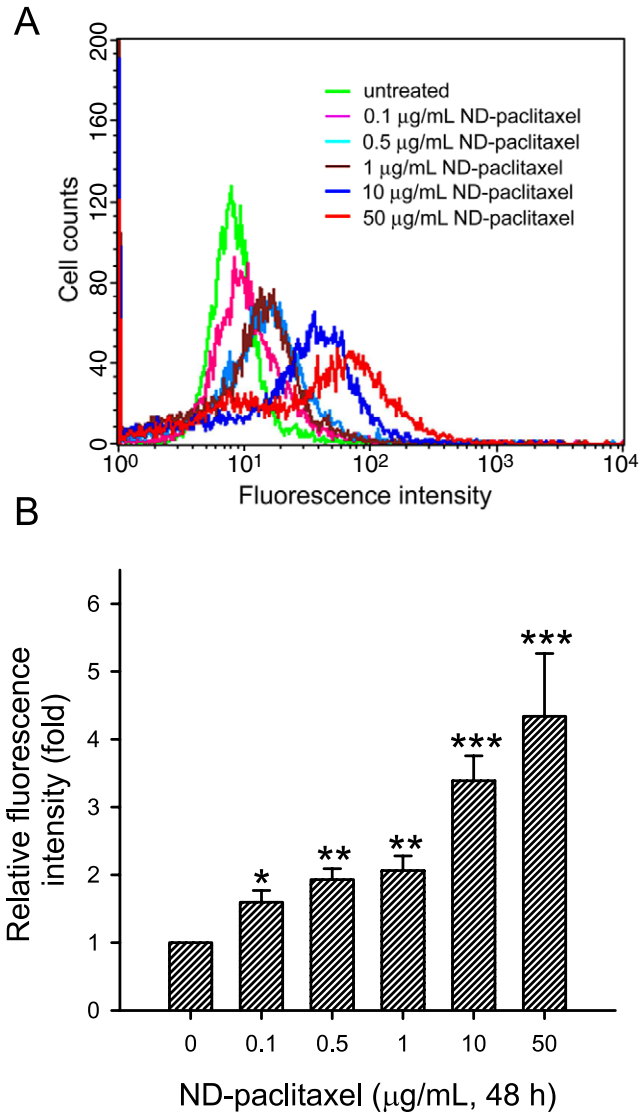

Figure 3. Uptake ability of ND-paclitaxel in human lung carcinoma cells. (A) A549 cells were treated with 0–50 μg ml^{-1} ND-paclitaxel for 48 h. At the end of treatment, the cells were trypsinized and then subjected to flow cytometer. (B) The fluorescence intensities were quantified by CellQuest software of the flow cytometer. Results were obtained from four separate experiments and the *bar* represents the mean ± S.E. $^{*}p < 0.05$, $^{**}p < 0.01$ and $^{***}p < 0.001$ indicate significant difference between untreated and ND-paclitaxel samples.

A549 lung carcinoma cells. Besides, the cross-section images of an ND-paclitaxel-treated A549 cell were captured under a laser scanning confocal microscope. Figure 5(A) shows that ND-paclitaxel particles were located on the microtubules and blocked the spindle formation. Nonetheless, NaOH-treated ND-paclitaxel particles did not block microtubules and were located in cytoplasm by dissection of confocal scanning of *Z* axis (figure 5(B)).

3.5. ND-paclitaxel induces the cell cycle arrest and apoptosis in lung carcinoma cells

To investigate the effect of ND-paclitaxel on the cell cycle progression, A549 cells were treated with ND-paclitaxel and analyzed by flow cytometer and mitotic index. Comparing with untreated and ND-treated samples, ND-paclitaxel dramatically decreased the G_1/G_0 fractions and increased the G_2/M fractions in A549 cells ($p < 0.01$) (figure 6(A)). The average percentages of G_2/M fractions were elevated to 83.4% after treatment with ND-paclitaxel by comparing with 23.0% before treatment (figure 6(A)). In untreated and ND-treated samples, the cells were divided into two daughter cells during cytokinesis; however, ND-paclitaxel blocked cell division and arrested in the prophase of mitosis (figure 6(B)). Furthermore, treatment with 0.1–50 μg ml^{-1} ND-paclitaxel for 48 h decreased the mitosis-regulated protein levels of CDC2 and phospho-CDC2 via a concentration-dependent manner in A549 cells (figure 7). Actin protein was an internal control protein, which was not altered by ND-paclitaxel. Additionally, the mitotic index was increased by treating with ND-paclitaxel but not in the untreated, ND alone and NaOH-treated ND-paclitaxel samples (figure 8(B)).

ND-paclitaxel also significantly increased the sub-G_1 fractions (apoptosis fractions) at the average value of 13.4% in A549 cells, but the sub-G_1 fractions of untreated or ND alone were at the basal level of 2–4% ($p < 0.01$) (figure 6(B)). Besides, we have confirmed and counted the percentage of apoptotic nuclear number by morphological changes under a fluorescence microscope. Consistently, ND-paclitaxel significantly elevated ∼12% apoptosis in A549 cells; in contrast, the NaOH-treated ND-paclitaxel lost the ability to increase the apoptosis level (figure 8(B)).

3.6. ND-paclitaxel inhibits tumorigenesis of human lung tumor xenograft in SCID mice

The model of a xenograft lung tumor in SCID mice was used to study the effect of ND-paclitaxel on anti-tumorigenesis. The xenograft lung tumor was developed in five-week-old SCID mice. After treatment with vehicle, ND or ND-paclitaxel in A549 lung carcinoma cells, mice received 1×10^6 cells by being subcutaneously injected. Figure 9(A) shows the visible lung tumors that were separated from sacrificed xenograft SCID mice. The tumors of mice were grown to an average 300–400 mm^3 in control and ND groups after inoculation for 70 days. Moreover, ND-paclitaxel dramatically reduced the tumor size at an average of ∼25 mm^3 (figure 9(B)). ND alone did not significantly alter the tumorigenesis of A549 cells in mice during 70 days' observation.

4. Discussion

Chemical drugs linked covalently with nanoparticles have been developed for diagnostic and therapeutic applications in recent years. Paclitaxel is a cancer chemotherapy drug, which blocks microtubules to mediate the mitotic arrest and cell death in cancer cells [29, 30]. Paclitaxel can stabilize microtubules and induces the formation of abnormal microtubule bundles to block the mitosis progression [29, 30]. In this study, we created a covalent linkage between ND and paclitaxel. ND-paclitaxel significantly induced the cell death in human lung carcinoma cells. ND-paclitaxel can be taken into lung cancer

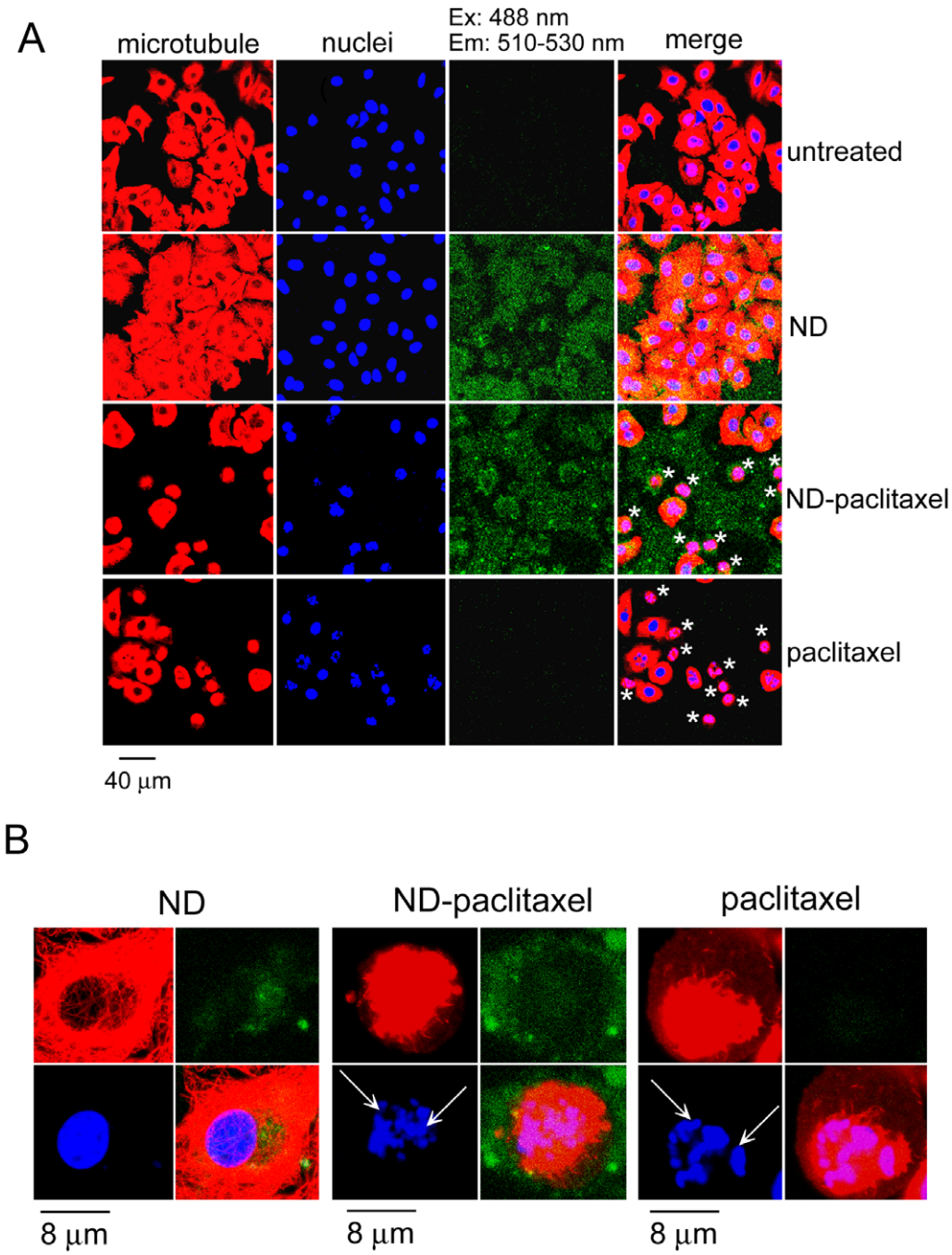

Figure 4. Effect of ND-paclitaxel on the induction of abnormal microtubules and chromosomes in human lung carcinoma cells. (A) A549 cells were treated with ND (50 μg ml^{-1} for 24 h), ND-paclitaxel (50 μg ml^{-1} for 24 h) or paclitaxel (50 nM, 24 h), and then subjected to cytoskeleton and nuclear staining. The microtubule proteins were stained with Cy3-labeled mouse anti-β-tubulin. The nuclei were stained with Hoechst 33258. Microtubules and nuclei exhibited red and blue colors, respectively. The green fluorescence from ND particles was excited by a wavelength of 488 nm and the emission was collected in the range 510–530 nm by using a confocal microscope. The stars indicate that the cell morphology (mitotic round-up) was affected by paclitaxel or ND-paclitaxel compared to untreated or ND-treated samples. (B) The pictures are amplified from (A). The arrows indicate the derangement of chromosomes after treatment with paclitaxel or ND-paclitaxel.

cells in a concentration-dependent manner. More importantly, ND-paclitaxel exerts its anticancer abilities by inducing mitotic arrest, apoptosis and anti-tumorigenesis. However, ND alone or denatured ND-paclitaxel did not induce the damage effects on lung cancer cells. The covalent linkage of nanoparticles and drugs provides an advantage for stabilization to avoid drug dissociation during the delivery process. We suggest that ND is a potential nanomaterial as a drug carrier for cancer drug delivery and therapy. Recently, it has been demonstrated that carbon nanotubes conjugated with paclitaxel exerted drug delivery for tumor suppression in mice [5]. Recently, Danhier *et al* reported that paclitaxel-loaded PEGylated PLGA-based

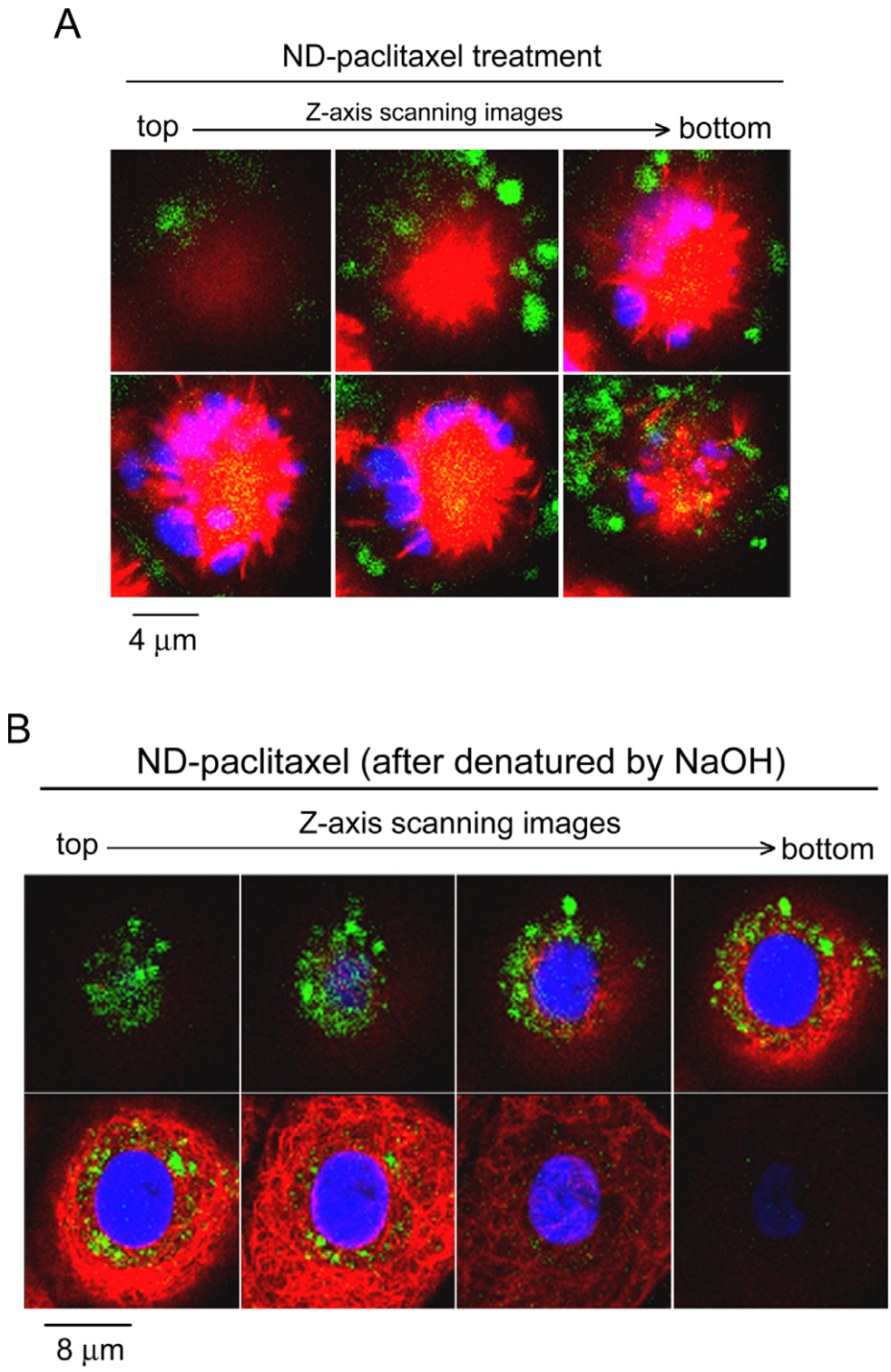

Figure 5. Location and distribution of ND-paclitaxel in human lung carcinoma cells. (A) An A549 cell from ND-paclitaxel (50 μg ml^{-1} for 24 h) treatment was visualized by examining Z-axis scanning images using a confocal microscope. The interaction of ND-paclitaxel with microtubules was observed by scanning in the vertical direction from top to bottom. Microtubules and nuclei exhibited red and blue colors, respectively. The green color shows the location of ND particles. The yellow color indicates that ND-paclitaxel particles were co-localized with microtubules. (B) An A549 cell from NaOH-treated ND-paclitaxel (50 μg ml^{-1} for 24 h) treatment was visualized by examining Z-axis scanning images of a confocal microscope.

nanoparticles displayed greater inhibition of tumorigenesis by comparison with paclitaxel [31]. Additionally, nanoliposomal delivery of cancer drugs have the benefits of prolonging drug in tissue residence during cancer therapy [6–8]. Therefore, nanoparticles provide the opportunities for improving cancer therapeutics by being conjugated with cancer drugs.

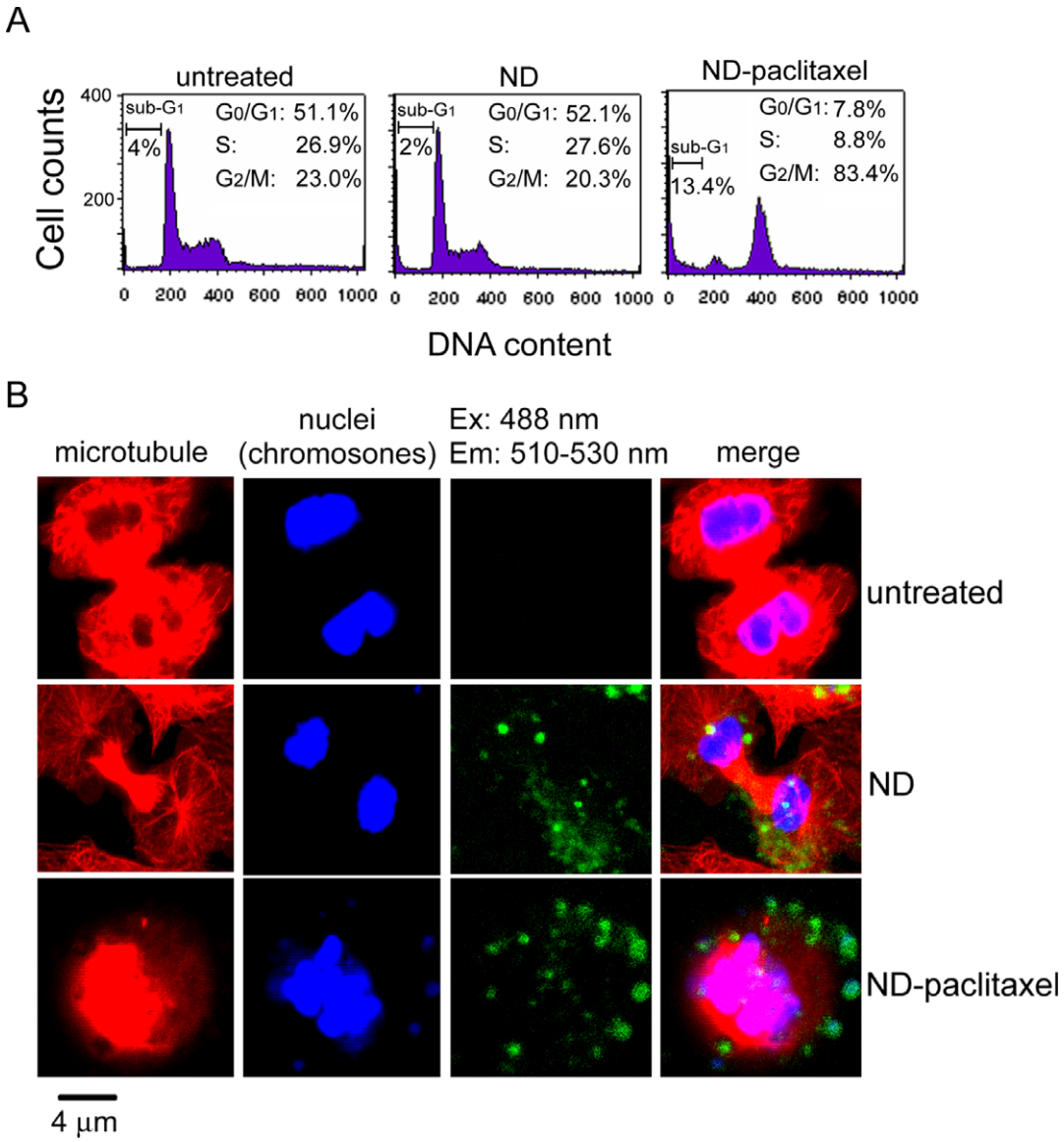

Figure 6. Effect of ND-paclitaxel on the cell cycle progression in human lung carcinoma cells. A549 cells were treated with 50 μg ml^{-1} ND or ND-paclitaxel for 24 h. (A) At the end of treatment, the A549 cells were trypsinized and then subjected to flow cytometry analyses. These data of each cell cycle phases and sub-G_1 fractions represented the average values from three separate experiments. (B) The β-tubulin and nuclei were stained with the Cy3-labeled mouse anti-β-tubulin and Hoechst 33258, respectively. Microtubules and nuclei exhibited red and blue colors, respectively. The green fluorescence from ND particles was excited by a wavelength of 488 nm and the emission was collected in the range 510–530 nm by using a confocal microscope. The untreated and ND-treated cells were separating into two daughter cells during cytokinesis. The ND-paclitaxel-treated cell was arrested in the prophase of mitosis.

The toxicity of nanoparticles is a critical issue of concern for clinical applications. Several studies showed that ND did not induce cytotoxicity in various cell types [11–16]. Recently, we have presented that ND particles are non-cytotoxic during cellular division and differentiation [12]. In the present study, ND particles did not elicit the mitotic blockage and apoptosis in lung cancer cells. Moreover, it is the first time demonstrating that ND particles did not influence the tumorigenesis of human lung cancer cells in xenograft SCID mice. In contrast, ND-paclitaxel is effective in inducing mitotic blockage, apoptosis and anti-tumorigenesis in lung cancer cells. Recently, it has been reported that no mice showed any symptoms of abnormality after intravenous injection of ND particles [17]. We propose that ND is a benign nanomaterial for drug delivery based on its non-cytotoxicity and biocompatibility.

ND powder produced by detonation synthesis has become available in large quantities, which has enabled many engineering applications [32, 33]. ND particles prepared by explosive techniques represent a novel class of nanomaterials possessing unique surface properties [34]. The surface of ND particles may be covered with a variety of functional groups, including carboxyl, lactone, ketone, hydroxyl and alkyl groups [35–37]. The ND-paclitaxel conjugation has been verified by atomic force microscope and NMR spectroscopy,

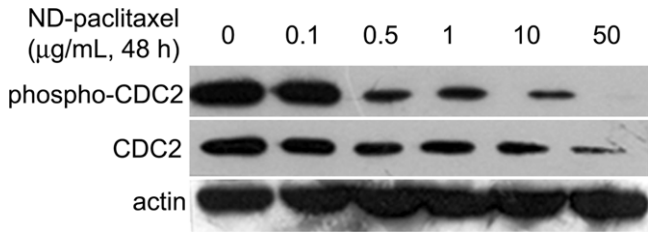

Figure 7. The effect of ND-paclitaxel on the protein levels of phospho-CDC2 and total CDC2 in human lung carcinoma cells. A549 cells were treated with or without ND (0.1–50 μg ml^{-1} for 48 h). The total protein extracts were subjected to Western blot analysis by using anti-phospho-CDC2, anti-CDC2 and actin antibodies. Representative Western blot results were shown from one of three separate experiments with similar findings.

and confirmed with infrared spectroscopy by the detection of deuterated paclitaxel. It has been shown that covalent immobilization of DNA on ND can be verified by diffuse reflectance infrared spectroscopy [20]. According to our experiments, we have developed a successful synthetic method for the covalent bonding of ND and paclitaxel. In our preliminary evaluation, we have estimated that each ND particle linked with ∼7 paclitaxel molecules (data not shown). After calculation, 1 μg ml^{-1} ND-paclitaxel contained ∼100 nM paclitaxel. 1 μg ml^{-1} ND-paclitaxel executed approximate 50% inhibition of cell survival in A549 cells. The 50% inhibition of cell survival by paclitaxel was ∼100 nM. These findings show that ND-paclitaxel is effective in inducing lung cancer cell death as well as paclitaxel. Accordingly, we have successfully synthesized a covalent bonding of ND-paclitaxel, which still preserves the anticancer activity of paclitaxel.

It has been shown that ND is detectable by its fluorescence property but without photobleaching [12, 14, 18]. We have examined the location and uptake ability of ND-paclitaxel in lung carcinoma cells by confocal microscopy and flow cytometry. Using confocal microscopy, we observed that ND-paclitaxel was taken into cancer cells and located in the microtubules and cytoplasm. ND particles can be taken into cells by endocytosis pathways such as clathrin-mediated endocytosis and macropinocytosis [12, 38]. Interestingly, we found that ND-paclitaxel uptake into cancer cells was in a concentration-dependent manner by flow cytometer analysis. The uptake ability of ND-paclitaxel is correlated to the anticancer activity of paclitaxel on inducing cell death and mitotic blockage in lung cancer cells. ND-paclitaxel has an ester bond between ND and paclitaxel that can be hydrolyzed by esterases. The ester linkage of ND-paclitaxel may be cleaved by esterases of lung carcinoma cells to release paclitaxel to execute microtubule inhibition and apoptosis. As a whole, the visualization, uptake ability and paclitaxel release of ND-paclitaxel contain advantages for cancer drug delivery.

In conclusion, we have synthesized a novel covalent linkage of ND and paclitaxel, which can be delivered into lung carcinoma cells. More importantly, the covalent bonding of ND-paclitaxel still preserves its anticancer activities on the mitotic blockage, apoptosis induction and anti-tumorigenesis in human lung carcinoma cells. We provide a functional ND-

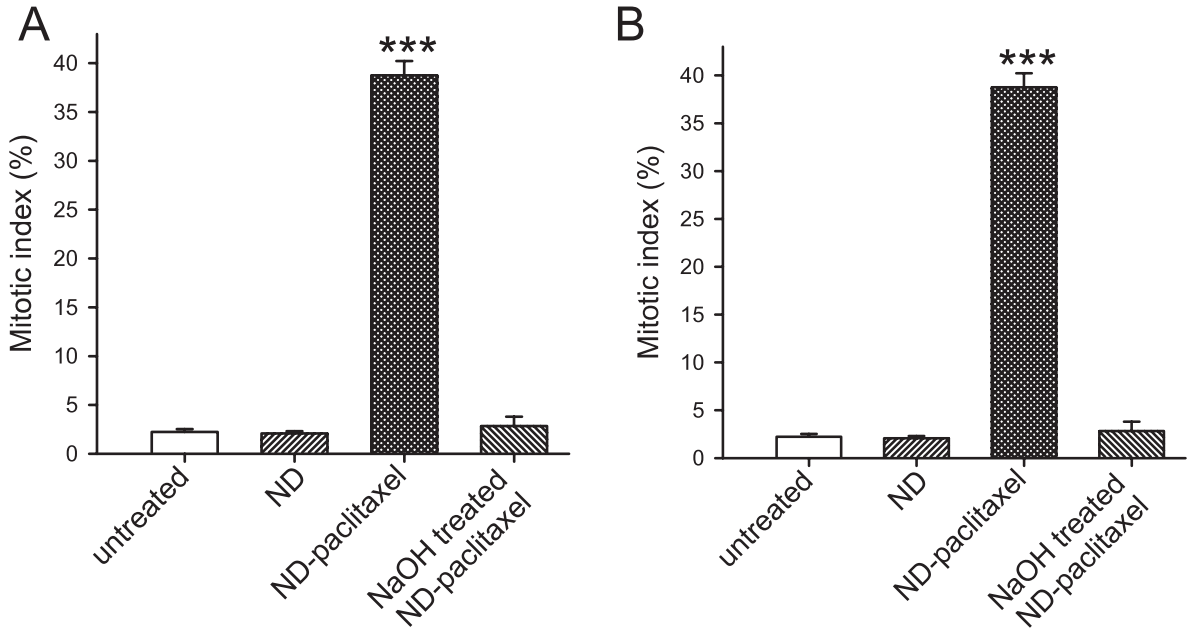

Figure 8. Effect of ND-paclitaxel on the percentages of mitotic index and apoptosis in human lung carcinoma cells. A549 cells were treated with 50 μg ml^{-1} ND, ND-paclitaxel or NaOH-treated ND-paclitaxel for 24 h. (A) After the end of treatment, the β-tubulin and nuclei were stained with the Cy3-labeled mouse anti-β-tubulin and Hoechst 33258, respectively. Mitotic index (the percentage of mitotic cell number/total cell number) was counted under a fluorescence microscope. (B) The percentage of apoptosis was counted by apoptotic nuclei. Results were obtained from three separate experiments and the bar represents the mean ± S.E. $^{**}p < 0.01$ and $^{***}p < 0.001$ indicate significant difference between the controls and ND-paclitaxel.

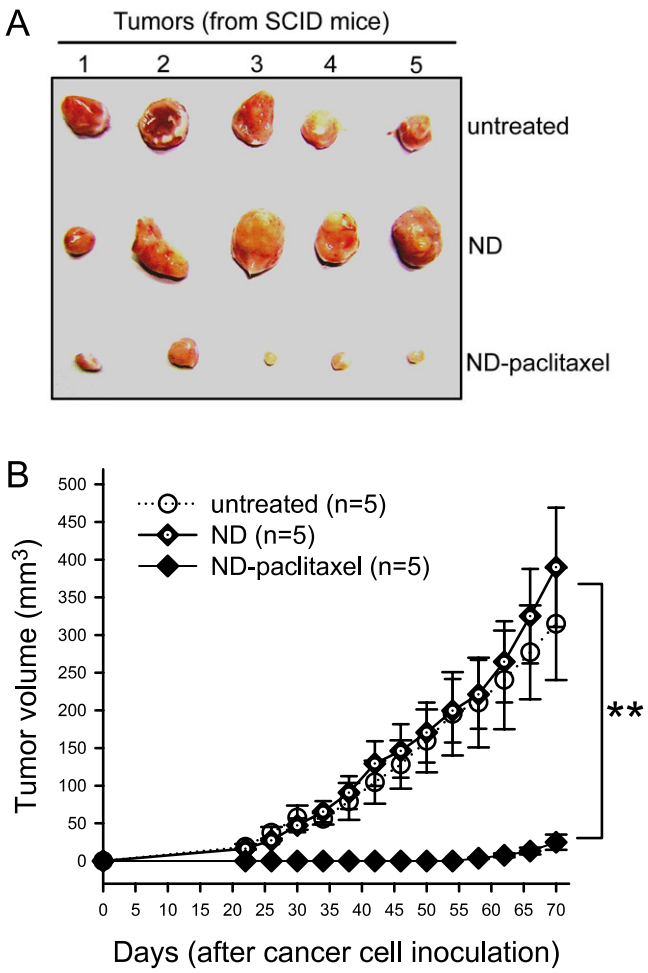

Figure 9. Effect of ND-paclitaxel on tumorigenesis of lung carcinoma tumor xenograft in SCID mice. (A) Xenograft lung tumor was developed in five-week-old CB17/Icr-Prkdc^{scid}/Crl mice. A549 cells were treated with ND or ND-paclitaxel (10 μg ml^{-1} for 48 h). Then the SCID mice were subcutaneously injected with 1×10^6 cells. Each group contained five mice. The visible lung tumors were separated from sacrificed xenograft mice after inoculation for 70 days. (B) The tumor volume and growth in SCID mice were measured by a digital caliper every four days until 70 days. Results were obtained from five mice per each group and the bar represents the mean $\pm$ S.E. $^{**}p < 0.01$ indicates significant difference between the controls and ND-paclitaxel.

paclitaxel conjugate developed for a novel strategy on cancer drug delivery and therapy.

Acknowledgments

This work was supported by grants from the National Science Council, ROC (NSC 96-2311-B-320-006-MY3, NSC 96-2113-M-259-001, NSC 96-2120-M-259-002 and NSC 97-2120-M-259-002) and financial support of the National Chiao-Tung University. The authors gratefully thank Tzu-Chi University (Hualien, Taiwan) for kindly providing the confocal microscope and flow cytometer.

References

[1] Michalet X, Pinaud F F, Bentolila L A, Tsay J M, Doose S, Li J J, Sundaresan G, Wu A M, Gambhir S S and Weiss S 2005 Quantum dots for live cells, *in vivo* imaging, and diagnostics *Science* **307** 538–44
[2] Gao X, Cui Y, Levenson R M, Chung L W and Nie S 2004 *In vivo* cancer targeting and imaging with semiconductor quantum dots *Nat. Biotechnol.* **22** 969–76
[3] Tada H, Higuchi H, Wanatabe T M and Ohuchi N 2007 *In vivo* real-time tracking of single quantum dots conjugated with monoclonal anti-HER2 antibody in tumors of mice *Cancer Res.* **67** 1138–44
[4] Akerman M E, Chan W C, Laakkonen P, Bhatia S N and Ruoslahti E 2002 Nanocrystal targeting *in vivo Proc. Natl Acad. Sci. USA* **99** 12617–21
[5] Liu Z, Chen K, Davis C, Sherlock S, Cao Q, Chen X and Dai H 2008 Drug delivery with carbon nanotubes for *in vivo* cancer treatment *Cancer Res.* **68** 6652–60
[6] Koshkina N V, Waldrep J C and Knight V 2003 Camptothecins and lung cancer: improved delivery systems by aerosol *Curr. Cancer Drug. Targets* **3** 251–64
[7] Noble C O, Krauze M T, Drummond D C, Yamashita Y, Saito R, Berger M S, Kirpotin D B, Bankiewicz K S and Park J W 2006 Novel nanoliposomal CPT-11 infused by convection-enhanced delivery in intracranial tumors: pharmacology and efficacy *Cancer Res.* **66** 2801–6
[8] Chou H H, Wang K L, Chen C A, Wei L H, Lai C H, Hsieh C Y, Yang Y C, Twu N F, Chang T C and Yen M S 2006 Pegylated liposomal doxorubicin (Lipo-Dox) for platinum-resistant or refractory epithelial ovarian carcinoma: a Taiwanese gynecologic oncology group study with long-term follow-up *Gynecol. Oncol.* **101** 423–8
[9] Service R F 2004 Nanotoxicology. Nanotechnology grows up *Science* **304** 1732–4
[10] Nel A, Xia T, Madler L and Li N 2006 Toxic potential of materials at the nanolevel *Science* **311** 622–7
[11] Liu K K, Cheng C L, Chang C C and Chao J I 2007 Biocompatible and detectable carboxylated nanodiamond on human cell *Nanotechnology* **18** 325102
[12] Liu K K, Wang C C, Cheng C L and Chao J I 2009 Endocytic carboxylated nanodiamond for the labeling and tracking of cell division and differentiation in cancer and stem cells *Biomaterials* **30** 4249–59
[13] Schrand A M, Huang H, Carlson C, Schlager J J, Omacr Sawa E, Hussain S M and Dai L 2007 Are diamond nanoparticles cytotoxic? *J. Phys. Chem.* B **111** 2–7
[14] Yu S J, Kang M W, Chang H C, Chen K M and Yu Y C 2005 Bright fluorescent nanodiamonds: no photobleaching and low cytotoxicity *J. Am. Chem. Soc.* **127** 17604–5
[15] Lechleitner T *et al* 2008 The surface properties of nanocrystalline diamond and nanoparticulate diamond powder and their suitability as cell growth support surfaces *Biomaterials* **29** 4275–84
[16] Chang I P, Hwang K C and Chiang C S 2008 Preparation of fluorescent magnetic nanodiamonds and cellular imaging *J. Am. Chem. Soc.* **130** 15476–81
[17] Yuan Y, Chen Y, Liu J H, Wang H and Liu Y 2009 Biodistribution and fate of nanodiamonds *in vivo Diamond Relat. Mater.* **18** 95–100
[18] Chao J I, Perevedentseva E, Chung P H, Liu K K, Cheng C Y, Chang C C and Cheng C L 2007 Nanometer-sized diamond particle as a probe for biolabeling *Biophys. J.* **93** 2199–208
[19] Yang W *et al* 2002 DNA-modified nanocrystalline diamond thin-films as stable, biologically active substrates *Nat. Mater.* **1** 253–7
[20] Ushizawa K, Sato Y, Mitsumori T, Machinami T, Ueda T and Ando T 2002 Covalent immobilization of DNA on diamond and its verification by diffuse reflectance infrared spectroscopy *Chem. Phys. Lett.* **351** 105–8

[21] Huang L C and Chang H C 2004 Adsorption and immobilization of cytochrome c on nanodiamonds *Langmuir* **20** 5879–84
[22] Cheng C Y, Perevedentseva E, Tu J S, Chung P H, Chenga C L, Liu K K, Chao J I, Chen P H and Chang C C 2007 Direct and *in vitro* observation of growth hormone receptor molecules in A549 human lung epithelial cells by nanodiamond labeling *Appl. Phys. Lett.* **90** 163903
[23] Krueger A, Stegk J, Liang Y, Lu L and Jarre G 2008 Biotinylated nanodiamond: simple and efficient functionalization of detonation diamond *Langmuir* **24** 4200–4
[24] Liu K K, Chen M F, Chen P Y, Lee T J F, Cheng C L, Chang C C, Ho Y P and Chao J I 2008 Alpha-bungarotoxin binding to target cell in a developing visual system by carboxylated nanodiamond *Nanotechnology* **19** 205102
[25] Shimkunas R A, Robinson E, Lam R, Lu S, Xu X, Zhang X Q, Huang H, Osawa E and Ho D 2009 Nanodiamond-insulin complexes as pH-dependent protein delivery vehicles *Biomaterials* **30** 5720–8
[26] Huang H, Pierstorff E, Osawa E and Ho D 2007 Active nanodiamond hydrogels for chemotherapeutic delivery *Nano Lett.* **7** 3305–14
[27] Zakharian T Y, Seryshev A, Sitharaman B, Gilbert B E, Knight V and Wilson L J 2005 A fullerene-paclitaxel chemotherapeutic: synthesis, characterization, and study of biological activity in tissue culture *J. Am. Chem. Soc.* **127** 12508–9
[28] Chao J I, Kuo P C and Hsu T S 2004 Down-regulation of survivin in nitric oxide-induced cell growth inhibition and apoptosis of the human lung carcinoma cells *J. Biol. Chem.* **279** 20267–76
[29] Schiff P B and Horwitz S B 1980 Taxol stabilizes microtubules in mouse fibroblast cells *Proc. Natl Acad. Sci. USA* **77** 1561–5
[30] Jordan M A, Toso R J, Thrower D and Wilson L 1993 Mechanism of mitotic block and inhibition of cell proliferation by taxol at low concentrations *Proc. Natl Acad. Sci. USA* **90** 9552–6
[31] Danhier F, Lecouturier N, Vroman B, Jerome C, Marchand-Brynaert J, Feron O and Preat V 2009 Paclitaxel-loaded PEGylated PLGA-based nanoparticles: *in vitro* and *in vivo* evaluation *J. Control Release* **133** 11–7
[32] Greiner N R, Phillips D S, Johnson J D and Volk F 1988 Diamonds in detonation soot *Nature* **333** 440–2
[33] Vereschagin A L, Sakovich G V, Komarov V F and Petrov E A 1993 Properties of ultrafine diamond clusters from detonation synthesis *Diamond Relat. Mater.* **3** 160–2
[34] Liu Y, Gu Z, Margrave J L and Khabashesku V N 2004 Functionalization of nanoscale diamond powder: fluoro-, alkyl-, amino-, and amino acid-nanodiamond derivatives *Chem. Mater.* **16** 3924–30
[35] Shenderova O V, Zhirnov V D and Brenner D 2002 Carbon nanostructures *Crit. Rev. Solid State Mater. Sci.* **27** 227–356
[36] Dolmatov V Y 2001 Detonation synthesis of ultradispersed diamonds: properties and applications *Russ. Chem. Rev.* **70** 607–26
[37] Ji S F, Jian T L, Xu K and Li S B 1998 FTIR study of the adsorption of water on ultradispersed diamond powder surface *Appl. Surf. Sci.* **133** 231–8
[38] Faklaris O, Garrot D, Joshi V, Druon F, Boudou J P, Sauvage T, Georges P, Curmi P A and Treussart F 2008 Detection of single photoluminescent diamond nanoparticles in cells and study of the internalization pathway *Small* **4** 2236–9